A computational gait model with a below-knee amputation and a semi-active variable-stiffness foot prosthesis

Michael A. McGeehan, PhD[1]; Peter G. Adamczyk, PhD[2]; Kieran M. Nichols, MS[2]; Michael E. Hahn, PhD[1]

Institutional Affiliations
[1]University of Oregon Department of Human Physiology
181 Esslinger Hall, 1525 University St.
Eugene, OR 97403
mmcgeeha@uoregon.edu, mhahn@uoregon.edu

[2]University of Wisconsin-Madison Department of Mechanical Engineering
Room 3039, Mechanical Engineering Building
1513 University Ave.
Madison, WI 53706-1539
peter.adamczyk@wisc.edu, knichols4@wisc.edu

Corresponding Author Information
Michael E. Hahn, PhD
University of Oregon, 181 Esslinger Hall, 1525 University St.
Eugene, OR 97403
(541) 346-3554
mhahn@uoregon.edu

Abstract

Introduction: Simulations based on computational musculoskeletal models are powerful tools for evaluating the effects of potential biomechanical interventions, such as implementing a novel prosthesis. However, the utility of simulations to evaluate the effects of varied prosthesis design parameters on gait mechanics has not been fully realized due to lack of a readily-available limb loss-specific gait model and methods for efficiently modeling the energy storage and return dynamics of passive foot prostheses. The purpose of this study was to develop and validate a forward simulation-capable gait model with lower limb loss and a semi-active variable-stiffness foot (VSF) prosthesis. **Methods**: A seven-segment 28-DoF gait model was developed and forward kinematics simulations, in which experimentally-observed joint kinematics were applied and the resulting contact forces under the prosthesis evolved accordingly, were computed for four subjects with unilateral below-knee amputation walking with a VSF. **Results**: Model-predicted resultant ground reaction force (GRF_R) matched well under trial-specific optimized parameter conditions (mean R^2: 0.97, RMSE: 7.7% body weight (BW)) and unoptimized (subject-specific, but not trial-specific) parameter conditions (mean R^2: 0.93, RMSE: 12% BW). Simulated anterior-posterior center of pressure demonstrated a mean $R^2 = 0.64$ and RMSE = 14% foot length. Simulated kinematics remained consistent with input data (0.23 deg RMSE, $R^2 > 0.99$) for all conditions. **Conclusions**: These methods may be useful for simulating gait among individuals with lower limb loss and predicting GRF_R arising from gait with novel VSF prostheses. Such data are useful to optimize prosthesis design parameters on a user-specific basis.

1. Introduction

Individuals with below-knee amputation who use prostheses for ambulation exhibit distinct gait characteristics, which may limit mobility and decrease quality of life. They may display gait asymmetry [1,2], elevated metabolic cost during locomotion [3], increased muscle activity [4], and a variety of psychological disorders including anxiety and depression [5]. Sustained prosthesis use may also lead to musculoskeletal injury through overloading of intact joints [6] and residual limb tissue damage due to pressure and shear forces at the prosthetic socket interface [7–9]. Each of these issues may be attenuated by improving user specificity in the design characteristics of foot prostheses. However, the effects of foot prosthesis design parameters (e.g. stiffness) are not well characterized, and thus achieving meaningful improvements in gait through prosthesis design has proven elusive [10,11]. In order to achieve improvements, a robust understanding of the relationships among anatomical morphologies associated with lower limb amputation (LLA), gait mechanics, and prosthesis design is necessary.

Gait simulations based on computational musculoskeletal models can be powerful tools to investigate human movement. Simulations have been used previously to evaluate musculoskeletal dynamics under a variety of conditions, including walking [12], running [13], and jumping [14]. However, the models used in these studies are not suitable for simulating gait among individuals with LLA, due to the altered lower limb mass, inertial properties and mechanical properties associated with a prosthetic foot and socket. LaPré et al. (2018) [15] and Willson et al. (2020) [16] developed limb loss-specific models in OpenSim [12], a popular musculoskeletal modeling and simulation platform. These studies used simulations to investigate the effects of prosthesis alignment and a biarticular clutched spring mechanism on gait mechanics, respectively. However, the models used in these studies do not account for the energy storage and return (ESR) properties of the prosthetic foot, thus limiting their ecological validity. Other studies that did incorporate the force and torque contributions of ESR feet into gait models focused on characterizing biomechanical and muscle activation responses with prosthesis use, but did not report systematic validation of the underlying gait and prosthesis models [17,18]. While these studies made important progress toward investigating the relationship among anthropometry, gait mechanics, and prosthetic foot design, they had limited ability to verify simulation results through comparison with experimental data. Due to these limitations, the use of simulations to inform the design of ESR foot prostheses has not been fully realized.

Previously, a reduced order computational model of a semi-active variable-stiffness foot (VSF) prosthesis [19] was developed and validated in [20]. However, there remains a need to integrate this model into a scalable forward kinematics and forward dynamics simulation capable gait model. Such a model would be useful for simulating gait and elucidating the relationships between ESR prosthesis design and gait mechanics on an individualized basis. The purpose of this study was to develop and validate a forward simulation-capable gait model with lower limb loss and a semi-active VSF.

2. Methods

2.1 Gait model design

A seven-segment, 28 degree-of-freedom (DoF) gait model (Figure 1) was developed in Simscape Multibody (Mathworks, Inc., Natick, MA). Simscape was chosen for its application to model-based design, customizability in simulation computing (e.g. differential equation solver profiles, numerical integration settings, and tolerance controls), and rich libraries of contact models, mechatronic components, and signal processing modules. Further, its integration with the rest of the Mathworks computational suite provides a link by which complex algorithms and data processing tools can be easily incorporated into the model.

The anatomical structures for the generic model were derived from open-source cadaveric skeletal 3D surface geometry data from Mitsuhashi et al. (2009) [21]. A massless head and torso (HAT) segment is included in the model for future uses; however, the present study utilized only kinematics of the pelvis and lower limbs. The pelvis interacts with the world frame via a 6-DoF bushing joint, which is the model's parent joint. For this study, pelvis translational movement in the frontal plane was prescribed using the experimental gait data described below in order to account for subjects that walked diagonally or performed minor turning during the gait trial. Other translational movements were unconstrained. Pelvis rotations in three planes with respect to the world frame were prescribed using experimental gait data. Each joint of the lower limb is modeled as a 3-DoF gimbal joint, with the coronal and axial rotations of the knee constrained to have no movement. Rotational movements in each plane may be constrained through user-defined inputs. To represent a below-knee amputation (BKA), the tibia and fibula were transected via a planar cut and encapsulated within a prosthetic socket. The residual limb and prosthetic socket were connected via a compliant bushing joint to assess 6 DoF socket-residual limb interface dynamics, similar to previous

work by LaPrè et al. (2018) [15]. The rotational and translational stiffness as well as displacement and velocity constraints were designed according to previous gait experiments [15] and finite element analysis [22]. The translational aspect of the bushing joint has a stiffness of 20 N/mm and damping of 10 N·s/mm. Vertical displacement of the residual limb with respect to the prosthetic socket (i.e. socket pitoning) is constrained to 35 mm maximum displacement and 100 mm/s maximum displacement velocity. The rotational aspect of the joint has a stiffness of 10 N·mm/deg and damping of 5 (N·mm)·s/deg The VSF model [20] is rigidly attached to the socket via a pylon and pyramid adapter using weld joints. Separate generic models with right and left side amputations were developed for this study and are available in the supplementary materials.

Methods for modeling the mechanical stiffness and ground contact dynamics of the VSF were previously described in [20]. Briefly, the VSF model was designed using the lumped parameter approach for approximating flexible body dynamics. The keel of the VSF is discretized into 16 segments connected with alternating revolute joints and weld joints, yielding eight DoF. The most posterior segment is 66 mm in length, which matches the minimum possible fulcrum position. The rest of the keel consists of 11.64-mm segments for a total beam length of 229 mm. The stiffness and damping values for the revolute joints were parameterized to represent the material properties of the VSF's G10/FR4 composite keel. A custom MATLAB script controls continuous fulcrum position (i.e. variable stiffness) between the posterior position at 66 mm and a maximum forward position of 151 mm. Stiffness of the VSF model was characterized by simulating static compression tests and optimizing the load-displacement response based on that of the physical VSF across the full range of fulcrum positions [19].

Segment masses were estimated according to DeLeva (1996) [23]. Mass distribution and inertial properties of the lower limbs and pelvis are modeled as conical frusta and an ellipsoid, respectively. The geometry of the conical frustum for each limb is defined using the proximal and distal joint radii for each segment, as derived from marker coordinates (see "Model scaling and parameterization"). The ellipsoid's radii are defined based on the distances between the right and left anterior and posterior superior iliac spines. The estimated mass of the HAT segment was added to the mass of the pelvis.

The model is designed with variant subsystems, which are Simscape coding structures that allow for multiple implementations of code where only one implementation is active during a simulation. In this design, gait simulations can be computed within a forward kinematics framework (i.e. joint kinetics and end effector positions estimated given joint kinematics as inputs) or forward dynamics framework (i.e. joint kinematics and end effector positions estimated given joint torques as inputs). Implementation of the variant subsystems (i.e. whether the model computes a forward kinematics or forward dynamics simulation) is controlled via user-defined inputs.

2.2 Model scaling and parameterization

Model scaling and parameterization are completed through a pipeline of custom MATLAB scripts (Figure 2). The pipeline uses raw marker coordinates from optical motion capture trials of subjects walking with the VSF to programmatically generate a scaled subject-specific gait model, parameterize the model, and drive forward gait simulations. First, data from a static capture trial are used to scale and assemble the generic gait model according to subject-specific anthropometrics. Estimates for segment dimensions, mass, and inertial properties are derived from the static data [23]. Then, the subject-specific gait model is used for subsequent forward kinematics or forward dynamics simulations to determine the movements or forces of the model based on inputs of joint angles or joint torques, respectively. Custom methods for signal processing and derivation of joint angles (e.g. Cardan-Euler sequences or quaternions) may be defined by the user. A variety of MATLAB-based approaches can be used to solve the model. These include both continuous and discrete options, an extensive set of ordinary differential equation (ODE) solvers, and a variety of numerical integration settings (e.g. fixed or variable time steps, step size constraints, and tolerance values). Each of these parameters may be strategically selected based on their suitability for a given simulation scenario, such as system dynamics, solution stability, computation speed, or solver robustness. The specific data processing and computational configurations used for simulations in this study are described in Section 2.4.

2.3 Contact model design and parameterization

Foot-ground contact models were designed for the VSF and the intact foot. A model of VSF-ground contact consists of 24 sphere-to-plane contact models [24] parameterized to represent the geometry and dynamics of the VSF's foam base. On the intact side, contact spheres were placed on anatomical locations that experience high localized pressure during stance phase (Figure 1) [25]. Methods for the design and parameterization of the contact model were previously described in [20]. Briefly, each contact sphere estimates normal (F_n) (eq. 1) and frictional (F_f) (eq. 2) forces associated with the collision of a viscoelastic sphere (a massless spring and damper system) and a

rigid plane [26,27]. For the intact foot, each contact sphere is parameterized independently according to Equations 1-2.

$$F_n = \begin{cases} (k * \delta^n) + y(b * \dot{\delta}) & \delta > 0, \dot{\delta} > 0 \\ k * \delta & \delta > 0, \dot{\delta} < 0 \\ 0 & \delta < 0 \end{cases} \quad (1)$$

$\boldsymbol{F_n}$: normal force
$\boldsymbol{k}$: contact stiffness
$\boldsymbol{\delta}$: penetration depth
$\boldsymbol{n}$: penetration exponent
$\boldsymbol{y}$: damping force scaling factor
$\boldsymbol{b}$: contact damping coefficient

$$F_f = \begin{cases} F_n * \mu_{static} & v_{poc} < v_{threshold} \\ F_n * \mu_{kinetic} & v_{poc} > v_{threshold} \end{cases} \quad (2)$$

$\boldsymbol{F_f}$: frictional force
$\boldsymbol{\mu}$: coefficient of friction
$\boldsymbol{v_{poc}}$: velocity at point of contact
$\boldsymbol{v_{threshold}}$: velocity threshold

For the VSF, the overall foot contact model was divided into five zones; the sphere-to-plane models were parameterized by zone (Figure 1). The heel of the VSF model is comprised of three zones; this choice was motivated by the sensitivity of contact parameters when few spheres are in contact with the walking plane (e.g. the heel of the foot early in stance phase). Contact parameters for each zone were optimized to match the experimental ground reaction force data from a sample trial using procedures described below. The foam base of the physical VSF undergoes compression throughout stance phase. To account for these effects, a modified Kelvin-Voigt nonlinear spring and damper force law (eq. (1)) was implemented to represent contact between the VSF and walking plane [26,27].

2.4 Gait simulations

The data presented in this study were derived via the processing and simulation pipeline described above. Forward kinematics gait simulations were computed for four subjects (one female) with a unilateral BKA (Table 1) walking with the VSF configured to "high", "medium", and "low" stiffness settings for three trials each (Table 2). To be included, participants must have been at least 2 years post-amputation and able to safely complete nine over-ground gait trials walking at 1.2 ± 0.1 m/s. Prior written informed consent was provided by all subjects as approved by the Health Sciences Institutional Review Board at the University of Wisconsin-Madison. All simulations were computed in Simscape Multibody using the *ode15s* solver profile with variable step sizes for numerical integration.

Motion capture (12-camera Optitrack Prime13 system, Natural Point, Inc. Corvallis, OR) and ground reaction force (GRF) data (Bertec Inc. Columbus, OH) collected from subjects during nine gait trials (Table 2), a static neutral pose, and functional joint movements [28] that were used to generate scaled subject-specific models and compute forward kinematics gait simulations. Marker coordinates and GRF data were sampled at 200 and 1000 Hz, respectively. Marker data were low-pass filtered (4th order Butterworth, f_c: 6 Hz). Force data were down-sampled (polynomial interpolation, f_s: 200 Hz) and low-pass filtered (4th order Butterworth, f_c: 40 Hz). Segment and joint kinematics were estimated using Cardan Euler rotation calculations in accordance with International Society of Biomechanics recommendations [29–31]. These data were then used to drive the corresponding joints in the model during simulations. Localized joint center coordinates were estimated for the hips, knees, and intact ankle joint using functional joint movements and methods described by Schwartz and Rozumalski (2005) [28]. The location of the pylon-pyramid adapter interface (i.e. prosthetic "ankle") was calculated based on a measured offset from markers placed on the VSF. This interface was assumed to be rigid. Motion at the socket-limb interface was considered to be passive based on the aforementioned velocity and displacement constraints. Residual limb length was estimated as the distance from the knee joint center to the base of the prosthetic socket and scaled accordingly. The mass and inertial properties of the residual limb were estimated first by deriving estimated density of the intact limb modeled as a conical frustum with an assigned mass estimated per De Leva (1996). The derived density of the intact limb was applied to the residual limb model, which was also modeled as a conical frustum. This limb was then truncated at the respective level of amputation for each subject.

Contact model parameters were optimized on a subject-specific basis. Contact model parameterization was formulated as a least-squares optimization problem with the objective of minimizing the sum of squared errors between model-predicted and experimentally measured resultant ground reaction force (GRF_R). For a description of the comparison between model-predicted and experimentally-measured data, see Section 2.5. A Latin Hypercube Sampling-based optimization algorithm was used to programmatically derive the stiffness, damping, and friction terms for each sphere. For each subject, contact model-derived GRF_R prediction was optimized using data from one medium stiffness trial. The GRF_R error resulting from this trial represents the theoretical optimal performance of the comprehensive VSF-ground contact model. The transferability of the optimized parameter values was determined by simulating the two remaining medium stiffness trials and the three remaining trials each for the low and high stiffness configurations. No GRF data were available to optimize or verify contact model parameters on the intact side. As such, stiffness and damping for contact spheres on the intact side were parameterized to simplify the model of the intact side, so that the contact spheres were able to support the model's mass throughout stance phase.

2.5 Gait model evaluation

The gait model's performance was evaluated under two scenarios: static and dynamic gait conditions. Of the three trials per condition (Table 2), Subject 2 did not complete one medium stiffness trial, and Subject 4 did not complete one high stiffness trial. In total, forward kinematics simulations were computed for 38 trials (4 static, and 34 dynamic). For the static condition, the model was simulated with anatomically neutral joint angles for ten seconds. Model-predicted GRF_R was measured at the end of the trial and compared to the mass of the subject. This comparison represents the accuracy of the contact parameters to estimate the ground contact force imparted by the subject with no dynamic component. For the dynamic conditions, forward kinematics gait simulations were computed for the nine gait trials per subject with high, medium, and low VSF stiffness configurations.

The Simscape solver computes the model's initial conditions by finding state values at the initial time step that exactly satisfy the model's system of equations. For all simulations in this study, the model conditions were assumed to start from steady state (i.e. zero derivative). The model was initialized in a posture taken from the experimental motion capture data at the first time step. The model's initial position in the gait environment was derived based on the initial coordinates of a virtual motion capture marker placed at the pelvis' origin frame. Then, joint kinematics, also from experimental data, were applied at each joint and the model was simulated forward in time, allowing kinematic movements and contact with the ground to evolve in time according to the model's dynamics. Continuous differential equations were integrated with respect to time to compute all model variables as a function of time. A forward kinematics-based approach was selected for this study because the goal was to apply experimentally-observed joint kinematics and allow the resulting contact forces under the prosthesis to evolve accordingly.

Joint kinematics and GRF_R data derived from simulations were low-pass filtered (4th order Butterworth: f_c: 6 Hz and 40 Hz, respectively). Simulation and experimental GRF_R were time locked and indexed to 0.25 s before and 0.25 s after stance phase. Including the brief period before and after stance phase provides insights regarding how the contact model behaves outside of stance phase and whether or not key gait events (e.g. heel strike and toe off) occur at similar time points in the simulated and experimental data. Resultant ground reaction force time series were re-sampled to 101 data points via cubic spline interpolation to allow for comparison between stance phases of differing lengths. Ensemble curves (mean ± SD) were generated for each condition. The cumulative impulse of GRF_R was calculated to verify the dynamic compatibility of the simulation with the measured GRF. The time integral of GRF_R has been shown previously to be indicative of whole-body kinetics [32].

Anterior-posterior center of pressure (CoP_{AP}) position was calculated as the weighted sum of each contact sphere's predicted normal force multiplied by its anterior-posterior position (x) (eq. (3)). Raw normal forces arising from each sphere during stance phase were low-pass filtered (4th order Butterworth: f_c: 40 Hz) and summed. Anterior-posterior CoP position was calculated throughout the stance phase. The CoP_{AP} time series data were low-pass filtered (4th order Butterworth: f_c: 6 Hz) and re-sampled to 101 data points via cubic spline interpolation to allow for comparison between stance phases of differing lengths. Joint kinematics, GRF_R, and CoP_{AP} derived from the simulations were compared to the corresponding data measured during experimental gait trials using coefficient of determination and RMSE.

$$\mathrm{CoP_{AP}} = \frac{\sum_{i=1}^{N} x_i F_{n_i}}{\sum F_n} \quad (3)$$

CoP_{AP}: Anterior-posterior center of pressure position

$\boldsymbol{x_i}$: Anterior posterior coordinate of contact sphere relative to the prosthesis heel (x = 0).

3. Results

In the static condition, model-predicted subject mass (from ground reaction force) matched the measured mass of each participant within 0.1%. In the dynamic conditions, simulated joint angles matched experimental joint angles well (mean RMSE: 0.14 ± 0.01 deg, mean R^2: 1.00 ± 0.00), indicating a successful forward-kinematics simulation. All simulated joint angles matched experimental values with less than 0.23 deg RMSE.

Optimization of the medium stiffness trial for each subject resulted in a mean GRF_R RMSE value of 7.7 ± 1.5% body weight (BW) and a mean R^2 of 0.97 ± 0.01 across stance phase (Figure 3). Cumulative impulse also matched well (RMSE: 0.76 ± 0.26% BW·s, R^2: 1.00 ± 0.00). In the time domain, model-predicted stance phases were, on average, 0.03 ± 0.03 s shorter compared to experimental data for this optimized trial.

In the unoptimized trials, experimental GRF_R and GRF_R impulse responses were similar in the time and amplitude domains across the three stiffness conditions (Figure 4). On average, stance phase times were 0.01 ± 0.01 s shorter in the simulations across the stiffness conditions. Time errors were least for the medium stiffness and greatest for the high stiffness simulations. Variability for GRF_R was greatest during the first 15% of stance phase for simulations and lowest for the experimental data during this time. The contact parameters optimized for the medium stiffness condition transferred well across the low and high stiffness conditions, which is evident by the similar RMSE values for GRF_R and GRF_R impulse (Table 3). Model-predicted GRF_R values were better in the high stiffness configuration, whereas predictions for GRF_R impulse were best in the medium and high stiffness conditions (Table 3).

Anterior-posterior CoP trajectory during stance phase was similar between simulated and experimental data (Figure 5, Table 3). However, divergent trajectories were observed, primarily between 15–40% of stance phase. Overall, RMSE values were 14 ± 4.4 percent foot length across all conditions, with the low stiffness condition performing the best. Simulated data exhibited a strong correlation ($R^2 > 0.70$) with experimental data for all stiffness conditions. Simulation-predicted CoP_{AP} showed similar variability compared to experimental data.

4. Discussion

The objective of this study was to develop and evaluate a forward simulation-capable gait model with below-knee amputation and a semi-active VSF prosthesis. The gait model and VSF-ground contact model were evaluated under static and dynamic gait conditions. Under static conditions, model-predicted mass exhibited an error < 0.01% with respect to the mass of the subjects. This value represents the performance of the contact model with no dynamic component. Under dynamic gait conditions, the ability of the model to predict GRF_R, GRF_R impulse, and COP_{AP} within a forward kinematics framework was evaluated. For all trials, simulated joint angles were strongly correlated with experimental angles ($R^2 > 0.999$ for all joints) with RMSE values of less than 0.23 deg for all joints. These values are logical for forward kinematics simulations, but importantly indicate that the model is numerically stable when actuated by joint kinematics measured during gait with the VSF. Further, concomitant agreement between the model's kinematic and kinetic response is critical for forward dynamics simulations of human gait.

Optimization of contact model parameters in the medium stiffness trials achieved a mean RMSE value of 7.5 ± 1.5 percent BW for GRF_R and 0.76 ± 0.26% BW·s for GRF_R impulse. These values represent the theoretical optimal performance of the comprehensive contact model within the present simulation framework. This contact model performance is similar to the values previously reported in biomechanical contact modeling work [33–35]. However, the focus of those studies was to predict foot-ground contact dynamics during gait for individuals with intact limbs. Direct comparison of these data was limited to work in intact limb biomechanical modeling due to a lack of studies reporting validation data for prosthesis-ground contact modeling in gait biomechanics. The strong correlation and low error for GRF_R impulse indicates that the contact model is able to predict the shape and trajectory of the GRF_R waveform arising from gait kinematics. Accurate prediction of GRF_R impulse is important for capturing whole-body energetics throughout gait [32]. The concomitant agreement for both simulated kinematics and kinetics further suggests that these methods are viable for simulating whole-body movement during gait.

The transferability of the optimized contact model parameters from the medium stiffness condition was assessed by simulating the two remaining medium stiffness trials and the six total trials with low and high stiffness configurations per subject. Compared to the optimized trials, error for simulation-derived GRF_R predictions increased by an average of 4% across the unoptimized trials. Mean GRF_R RMSE and R^2 were 12.7 ± 6.9% BW and 0.91 ± 0.02 respectively for the remaining medium stiffness trials. These errors were slightly greater than those for the low and high stiffness trials (Table 3). There was one outlier trial for the medium stiffness condition, classified as a RMSE response greater than three standard deviations from the mean. This trial was not removed from the mean values presented in Figures 3 and 5 and Table 3, since it could not be discerned what the source of the increased error was. With this trial removed, the model's GRF_R response for the medium stiffness was 9.6 ± 2.6% BW RMSE and 0.96 ± 0.01 R^2. The same subject had a single high error trial in the low and high stiffness

conditions. However, these trials did not meet the criteria for outlier classification and hence were included. Data from these trials show a brief but large overshoot (>1 BW) for model-predicted GRF_R at initial heel contact. Each of these trials likely contributed to the higher mean error and variability in model-predicted GRF_R early in stance phase (Figure 4). Given that the outlier trials were all from the same subject, these errors may be due to errors or noise in the kinematic data used to drive the model. Errors early in stance phase could be compounded by the relative sensitivity of contact model parameters when a single sphere is in contact with the walking surface.

Model-predicted stance phase times agreed well with experimental values. On average, simulated stance phases were 0.01 ± 0.01 s shorter than experimental times. Errors were similar between stiffness conditions. Accurate prediction of stance phase length is important because it contributes to the model's ability to quantify metrics such as the time integral of GRFs, which may be indicative of whole-body kinetics [32]. Presented by increasing stiffness condition, experimentally-measured stance phase times were 0.68 ± 0.06, 0.72 ± 0.06, and 0.71 ± 0.07 s.

Simulated CoP_{AP} values were strongly correlated ($R^2 > 0.70$) with experimental data in all stiffness conditions. The RMSE values achieved using this model were similar to those reported in a previous study [36], which used a subject-specific 38 contact point model to predict CoP_{AP} for individuals with intact limbs. Accurate mapping of CoP_{AP} throughout stance phase is vital for simulating the effects of variable prosthesis stiffness on joint forces and moments during gait. Errors in model-predicted CoP_{AP} may be reduced by increasing the density of contact spheres distributed on the plantar surface of the foot, which would improve the resolution of CoP_{AP} predictions. However, this would likely result in increased execution time for simulations due to increased model complexity and also increase complexity of the contact parameter optimization problem. The low density of contact spheres in the heel of the VSF model is a likely source of the steep inflection in the CoP_{AP} trajectory early in stance phase, which contrasts the more gradual progression depicted in the experimental data (Figure 5).

Computation times are an important consideration in simulation-based approaches. Previous work has shown the lumped parameter approach for modeling ESR prosthesis dynamics to be more computationally efficient compared to more detailed finite element models [20]. Total execution times for the gait model were 13.7 ± 2.48, 16.8 ± 4.66, and 64.3 ± 71.2 times slower than real time for the low, medium, and high stiffness conditions. Increased execution times for the stiff conditions are a reflection of the need for small time-steps in solving a rapidly-evolving, stiff differential equation. Computation times were also increased for participants with more mass. These times could be reduced by utilizing "Accelerator" or "Rapid Accelerator" modes in Simscape Multibody, which improve simulation times by generating a C-code executable of the model. For example, one subject's simulations computed 60% faster in Accelerator mode compared to Normal mode across the nine trials. Rapid Accelerator mode was not tested in this study. All simulations were performed on a quad-core computer with a 4.0 GHz processor.

The present data show promise for predicting GRF_R arising from gait with a semi-active VSF prosthesis. These methods may be applied to the design and prescription of lower limb prostheses and forward dynamics simulations in robotics and biomechanics. For example, simulations could be used to evaluate the potential effects of varied prosthesis design parameters on the gait mechanics of a user. Simulations could also be computed within an optimal control framework to identify optimal device configurations and manufacture customized prostheses. Evaluating these effects within a simulation-based framework rather than traditional *in vivo* experimentation minimizes risk and time spent by the user. Further, a broad spectrum of prosthesis design parameters could be modeled and simulated without the need to manufacture multiple devices or the costs associated with doing so. Within biomechanics, simulated stiffness could be varied to minimize a biomechanical cost function such as peak or average joint moment or metabolic cost. Further optimization of the VSF-ground contact model may be necessary for simulation scenarios with error tolerances less than 12% BW (Table 3). Similar improvements may be required if the mean difference between simulation conditions is less than the error of the model, as was the case for the variation in GRF_R by VSF stiffness condition presented in this study. Reducing error in model-predicted GRF_R may be accomplished through improved methods in optimizing contact model parameters. For example, the objective function could be evaluated under a variety of conditions, thereby improving the generalizability of the contact model. A deformable contact model, such as presented in Jackson, Hass, and Fregly (2016), may also be a viable means of representing foam deformation throughout stance phase and thus reducing error.

Previous work in gait simulations with biomechatronic devices has often relied on abstract representations of components such as motors, electronics, and control systems [16,37,38]. In contrast, Simscape Multibody and Simulink offer a large library of these components, which can be readily integrated into the model for more realistic representations of biomechatronic systems. Further, control system parameters derived from simulations can be readily deployed to prototype devices. As such, this model may be advantageous for simulating gait with biomechatronic devices.

These methods assume accurate estimation of segment length, joint centers, and joint angles which were derived from marker-based motion capture data. Each of these metrics likely suffers from small errors due to marker placement, localization, and coordinate system design. Such errors would contribute to decrements in contact model performance. Characterizing the model's sensitivity to varied joint kinematics is possible within the present simulation paradigm. However, this analysis was not performed due to lack of experimental gait data necessary to quantify accuracy of those simulations.

The components and joints of the prosthetic limb were also modeled as rigid, which may not be completely accurate to represent the physical limb. This discrepancy would manifest as small differences in kinematics and energy transfer between the components of the prosthetic limb. Nevertheless, simulated motions were consistent with experimental data of subjects walking with the VSF and other previously reported data of spatiotemporal gait patterns among persons with lower limb loss [39,40]. Another limitation is inherent to the reduced order design of the lumped parameter VSF keel, which constrains keel motion to the sagittal plane. While this design is computationally efficient compared to more detailed finite element models, it fails to account for small torsional keel motions that would be possible under ecological gait conditions with the physical VSF. Future work could develop a lumped parameter model that allows for torsional keel movement in the frontal plane. Within the gait model, future work should incorporate biologically-inspired muscle models (e.g. Hill [41] or Thelen [42] models) to actuate joints for forward dynamics simulations. This would improve the biomechanical and physiological validity of the model and also allow for neuromuscular evaluation of simulated gait.

5. **Conclusions**

The present study demonstrates that the ESR properties of a semi-active VSF can be modeled and integrated into a scalable gait model that accounts for altered lower limb mass and inertial properties associated with LLA. The model captured whole-body kinetics associated with gait with varied prosthesis stiffnesses. Foot-ground contact models were used to estimate GRF_R with 7.7% BW mean RMSE in optimized gait trials, which translated to a mean RMSE of 12% across unoptimized trials. The contact models also predicted COP_{AP} with RMS error of 14% foot length. This model performance may be sufficient for gait simulations among persons with lower limb loss. Such simulations may be used to aid in the prosthesis design and prescription process in order to improve user mobility. These methods may also be helpful to identify other important prosthesis design parameters, which can be modified to optimize gait. Further contact model optimization and error reduction may be required for simulation-based comparisons of varied prosthesis stiffness, where differences in GRF_R magnitude may be nuanced.

Statement of acknowledgements: The authors would like to thank Evan Glanzer for his work in developing and testing the variable-stiffness foot and Terry Denery for his intellectual contributions in optimizing the contact model.

Funding sources: This work was funded in part by the Lokey Doctoral Science Fellowship (MAM) and NIH grant HD074424 (PGA).

403

Acronyms widely used in text

BKA	Below-Knee Amputation
BW	Body Weight; M*g
CoP	Center of Pressure
DoF	Degrees of Freedom
ESR	Energy Storage and Return
GRF_R	Resultant Ground Reaction Force, N; $\sqrt{GRF_X{}^2 + GRF_y{}^2 + GRF_z{}^2}$
LHS	Latin Hypercube Sampling
LLA	Lower Limb Amputation
ode15s	Ordinary differential equation 15 solver
SD	Standard Deviation
RMSE	Root Mean Square Error; $\sqrt{\frac{\sum_{i=1}^{N}(Experimental_i - Simulation_i)^2}{N}}$
VSF	Variable Stiffness Foot

Abbreviations

a	Overhung length, mm
b	Damping coefficient, N·s/mm
B	Support fulcrum position, mm
D	Displacement, mm
F	Force, N
k	Linear stiffness, N/mm
L	Total beam length, mm
l	Supported length, mm
n	Penetration exponent
R^2	Coefficient of determination
μ	Coefficient of friction
v	Linear velocity, mm/s
y	Scaling factor
δ	Penetration depth, mm
$\dot{\delta}$	Penetration velocity, mm/s
ω	Angular velocity, rad/s

Superscripts and subscripts

CoP_{AP}	Anterior-posterior (Center of Pressure)
F_f	Frictional force, N
F_n	Normal force, N
GRF_R	Resultant ground reaction force, N
v_{poc}	Linear velocity at point of contact, mm/s
$v_{threshold}$	Linear velocity threshold, mm/s
$\mu_{kinetic}$	Coefficient of kinetic friction
μ_{static}	Coefficient of static friction

404

[1] Schaarschmidt, M., Lipfert, S. W., Meier-Gratz, C., Scholle, H. C., and Seyfarth, A., 2012, "Functional Gait Asymmetry of Unilateral Transfemoral Amputees," Hum. Mov. Sci., **31**(4), pp. 907–917.

[2] Sanderson, D. J., and Martin, P. E., 1997, "Lower Extremity Kinematic and Kinetic Adaptations in Unilateral Below-Knee Amputees during Walking," Gait Posture, **6**(2), pp. 126–136.

[3] van Schaik, L., Geertzen, J. H., Dijkstra, P. U., and Dekker, R., 2019, "Metabolic Costs of Activities of Daily Living in Subjects with Lower Limb Amputation: A Systematic Review and Meta-Analysis. Article Submitted for Publication," PLoS One, **14**(3), p. e0213256.

[4] Fey, N. P., Klute, G. K., and Neptune, R. R., 2013, "Altering Prosthetic Foot Stiffness Influences Foot and Muscle Function during Below-Knee Amputee Walking: A Modeling and Simulation Analysis," J. Biomech., **46**, pp. 637–644.

[5] Mckechnie, P. S., and John, A., 2014, "Anxiety and Depression Following Traumatic Limb Amputation: A Systematic Review.," Injury, **45**(12), pp. 1859–66.

[6] Gailey, R., Allen, K., Castles, J., Kucharik, J., and Roeder, M., 2008, "Review of Secondary Physical Conditions Associated with Lower-Limb Amputation and Long-Term Prosthesis Use," JRRD, **45**(1), pp. 15–30.

[7] Sanders, J. E., and Daly, C. H., 1993, "Measurement of Stresses in Three Orthogonal Directions at the Residual Limb-Prosthetic Socket Interface," IEEE Trans. Rehabil. Eng., **1**(2), pp. 79–85.

[8] Al-Fakih, E. A., Abu Osman, N. A., and Mahmad Adikan, F. R., 2016, "Techniques for Interface Stress Measurements within Prosthetic Sockets of Transtibial Amputees: A Review of the Past 50 Years of Research," Sensors (Switzerland), **16**(7).

[9] Courtney, A., Orendurff, M. S., and Buis, A., 2016, "Effect of Alignment Perturbations in a Trans-Tibial Prosthesis User: A Pilot Study," J. Rehabil. Med., **48**(4), pp. 396–401.

[10] Casillas, J. M., Dulieu, V., Cohen, M., Marcer, I., and Didier, J. P., 1995, "Bioenergetic Comparison of a New Energy-Storing Foot and SACH Foot in Traumatic below-Knee Vascular Amputations.," Arch. Phys. Med. Rehabil., **76**(1), pp. 39–44.

[11] Postema, K., Hermens, H. J., De Vries, J., Koopman, H. F. J. M., and Eisma, W. H., 1997, "Energy Storage and Release of Prosthetic Feet Part 1: Biomechanical Analysis Related to User Benefits," Prosthet. Orthot. Int., **21**, pp. 17–27.

[12] Rajagopal, A., Dembia, C. L., DeMers, M. S., Delp, D. D., Hicks, J. L., and Delp, S. L., 2016, "Full-Body Musculoskeletal Model for Muscle-Driven Simulation of Human Gait.," IEEE Trans. Biomed. Eng., **63**(10), pp. 2068–79.

[13] Seth, A., Sherman, M., Reinbolt, J. A., and Delp, S. L., 2011, "OpenSim: A Musculoskeletal Modeling and Simulation Framework for in Silico Investigations and Exchange," Procedia IUTAM, **2**(2), pp. 212–232.

[14] Porsa, S., Lin, Y.-C., and Pandy, M. G., 2015, "Direct Methods for Predicting Movement Biomechanics Based Upon Optimal Control Theory with Implementation in OpenSim," Ann. Biomed. Eng., **44**(8), pp. 2542–2557.

[15] LaPrè, A. K., Price, M. A., Wedge, R. D., Umberger, B. R., and Sup, F. C., 2018, "Approach for Gait Analysis in Persons with Limb Loss Including Residuum and Prosthesis Socket Dynamics," Int. j. numer. method. biomed. eng., **34**(4), p. e2936.

[16] Willson, A. M., Richburg, C. A., Czerniecki, J., Steele, K. M., and Aubin, P. M., 2020, "Design and Development of a Quasi-Passive Transtibial Biarticular Prosthesis to Replicate Gastrocnemius Function in Walking," J. Med. Device., **14**(2), p. 025001.

[17] Fey, N. P., Klute, G. K., and Neptune, R. R., 2012, "Optimization of Prosthetic Foot Stiffness to Reduce Metabolic Cost and Intact Knee Loading During Below-Knee Amputee Walking: A Theoretical Study," J. Biomech. Eng., **134**, pp. 111005-1–10.

[18] Russel Esposito, E., and Miller, R. H., 2018, "Maintenance of Muscle Strength Retains a Normal Metabolic Cost in Simulated Walking after Transtibial Limb Loss," PLoS One, **13**(1), pp. 1–19.

[19] Glanzer, E. M., and Adamczyk, P. G., 2018, "Design and Validation of a Semi-Active Variable Stiffness Foot Prosthesis," IEEE Trans. Neural Syst. Rehabil. Eng., **26**(12), pp. 2351–2359.

[20] McGeehan, M., Adamczyk, P., Nichols, K., and Hahn, M., 2021, "A Reduced Order Computational Model of a Semi-Active Variable-Stiffness Foot Prosthesis." *Journal of Biomechanical Engineering*. In press.

[21] Mitsuhashi, N., Fujieda, K., Tamura, T., Kawamoto, S., Takagi, T., and Okubo, K., 2009, "BodyParts3D: 3D Structure Database for Anatomical Concepts," Nucleic Acids Res., **37**(Database), pp. D782–D785.

[22] Jia, X., Zhang, M., and Lee, W. C. C., 2004, "Load Transfer Mechanics between Trans-Tibial Prosthetic Socket and Residual Limb - Dynamic Effects," J. Biomech., **37**, pp. 1371–77.

[23] De Leva, P., 1996, "Adjustments to Zatsiorsky-Seluyanov's Segment Inertia Parameters," J. Biomech.,

29(9), pp. 1223–1230.
[24] Miller, S., 2020, "Simscape Multibody Contact Forces Library."
[25] Lugade, V., and Kaufman, K., 2014, "Center of Pressure Trajectory during Gait: A Comparison of Four Foot Positions," Gait Posture, **40**(4), pp. 719–722.
[26] Shourijeh, M. S., and McPhee, J., 2015, "Foot–Ground Contact Modeling within Human Gait Simulations: From Kelvin–Voigt to Hyper-Volumetric Models," Multibody Syst. Dyn., **35**(4), pp. 393–407.
[27] Lemaitre, J., 2001, *Handbook of Materials Behavior Models*, Academic Press.
[28] Schwartz, M. H., and Rozumalski, A., 2005, "A New Method for Estimating Joint Parameters from Motion Data," J. Biomech., **38**, pp. 107–116.
[29] Grood, E. S., and Suntay, W. J., 1983, "A Joint Coordinate System for the Clinical Description of Three-Dimensional Motions: Application to the Knee.," J. Biomech. Eng., **105**(2), pp. 136–44.
[30] Wu, G., Siegler, S., Allard, P., Kirtley, C., Leardini, A., Rosenbaum, D., Whittle, M., D'Lima, D. D., Cristofolini, L., Witte, H., Schmid, O., and Stokes, I., 2002, "ISB Recommendation on Definitions of Joint Coordinate System of Various Joints for the Reporting of Human Joint Motion - Part I: Ankle, Hip, and Spine," J. Biomech., **35**(4), pp. 543–548.
[31] Wu, G., and Cavanagh, P. R., 1995, "ISB Recommendations For the Standardized Reporting In Kinematic Data," J. Biomech., **28**(10), pp. 1257–1261.
[32] Peterson, C. L., Kautz, S. A., and Neptune, R. R., 2011, "Braking and Propulsive Impulses Increase with Speed during Accelerated and Decelerated Walking," Gait Posture, **33**(4), pp. 562–567.
[33] Van Hulle, R., Schwartz, C., Denoël, V., Croisier, J.-L., Forthomme, B., and Brüls, O., 2020, "A Foot/Ground Contact Model for Biomechanical Inverse Dynamics Analysis," J. Biomech., **100**(2020).
[34] Lopes, D. S., Neptune, R. R., Ambrósio, J. A., and Silva, M. T., 2015, "A Superellipsoid-Plane Model for Simulating Foot-Ground Contact during Human Gait," Comput. Methods Biomech. Biomed. Engin., pp. 1–10.
[35] Brown, P., and McPhee, J., 2018, "A 3D Ellipsoidal Volumetric Foot–Ground Contact Model for Forward Dynamics," Multibody Syst. Dyn., **42**(4), pp. 447–467.
[36] Jackson, J. N., Hass, C. J., and Fregly, B. J., 2016, "Development of a Subject-Specific Foot-Ground Contact Model for Walking," J. Biomech. Eng., **138**(9), pp. 091002-1–12.
[37] Dembia, C. L., Silder, A., Uchida, T. K., Hicks, J. L., and Delp, S. L., 2017, "Simulating Ideal Assistive Devices to Reduce the Metabolic Cost of Walking with Heavy Loads," PLoS One, **12**(7).
[38] Khamar, M., Edrisi, M., and Zahiri, M., 2019, "Human-Exoskeleton Control Simulation, Kinetic and Kinematic Modeling and Parameters Extraction," MethodsX, **6**, pp. 1838–1846.
[39] Winter, D. A., and Sienko, S. E., 1988, "Biomechanics of Below-Knee Amputee Gait," J. Biomech., **21**(5), pp. 361–367.
[40] Su, P.-F., Gard, S. A., Lipschutz, R. D., and Kuiken, T. A., 2008, "Differences in Gait Characteristics Between Persons With Bilateral Transtibial Amputations, Due to Peripheral Vascular Disease and Trauma, and Able-Bodied Ambulators," Arch Phys Med Rehabil, **89**(7), pp. 1386–1394.
[41] Hill, A., 1938, "The Heat of Shortening and the Dynamic Constants of Muscle," Proc. R. Soc. London. Ser. B - Biol. Sci., **126**(843), pp. 136–195.
[42] Thelen, D. G., 2003, "Adjustment of Muscle Mechanics Model Parameters to Simulate Dynamic Contractions in Older Adults," J. Biomech. Eng., **125**(1), pp. 70–77.

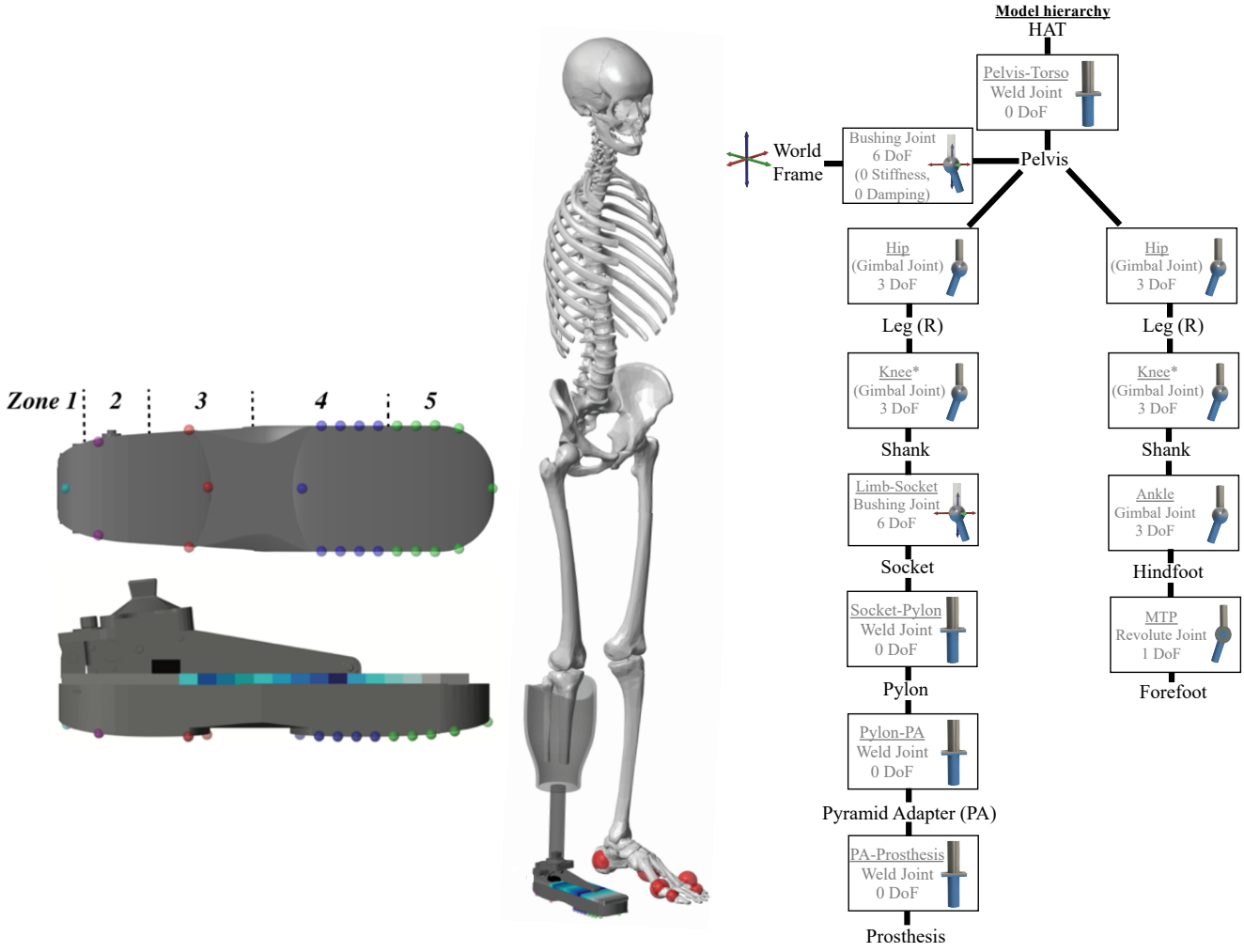

Figure 1: **[Left]**: Model of the VSF. The discretization of the VSF's keel is represented through the color gradient. The fulcrum (black rectangle) can be positioned from 66 mm (shown) to 151 mm from the posterior end. **[Center]**: Generic anatomic gait model with a right side below-knee amputation. Sphere-to-plane contact models are depicted in red (intact side) and multi-color (VSF side). **[Right]**: Generic gait model hierarchy. Parameters are mirrored for the model with a left side amputation. *Knee motion was constrained to the sagittal plane for simulations in this study. **PA**: Pyramid adapter, **MTP**: Metatarsophalangeal joint.

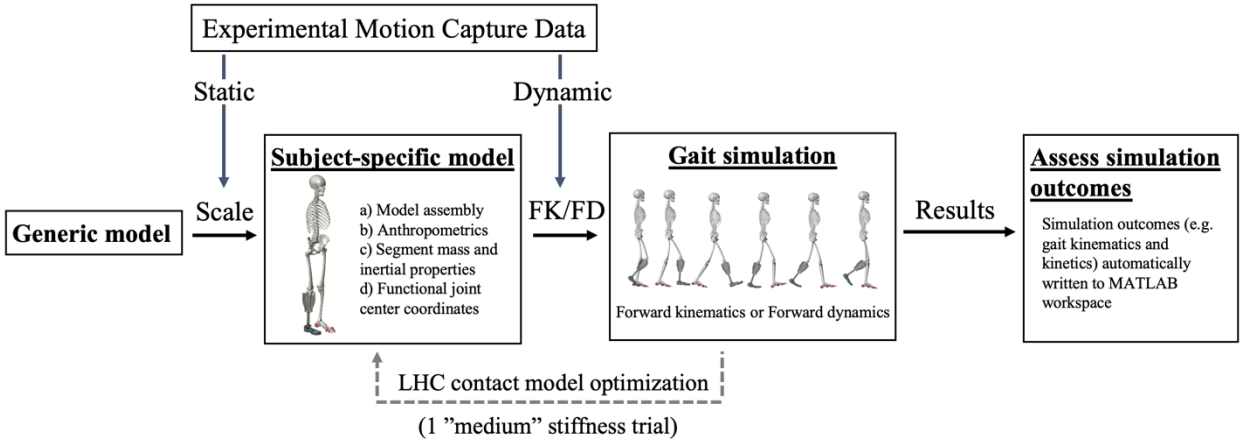

Figure 2: Overview of data processing and model parameterization pipeline. **FK**: Forward kinematics, **FD**: Forward dynamics.

Table 1: Participant characteristics

Subject	Sex	Age (y)	Height (cm)	Mass (kg)	Amputation side	Years post-amputation
1	Male	34	181	77.3	Right	15
2	Male	51	175	111	Right	8
3	Male	70	180	83.8	Left	14
4	Female	61	163	63.8	Right	8
Mean ± SD	–	54 ± 15	175 ± 19.9	84.0 ± 19.9	–	11 ± 3.8

Table 2: Summary of experimental trials.

Number of trials	VSF condition (Forefoot stiffness)	Gait condition
3	"High" stiffness (32 N/mm)	1.2 ± 0.1 m/s, over ground walking
3	"Medium" stiffness (19 N/mm)	1.2 ± 0.1 m/s, over ground walking
3	"Low" stiffness (10 N/mm)	1.2 ± 0.1 m/s, over ground walking

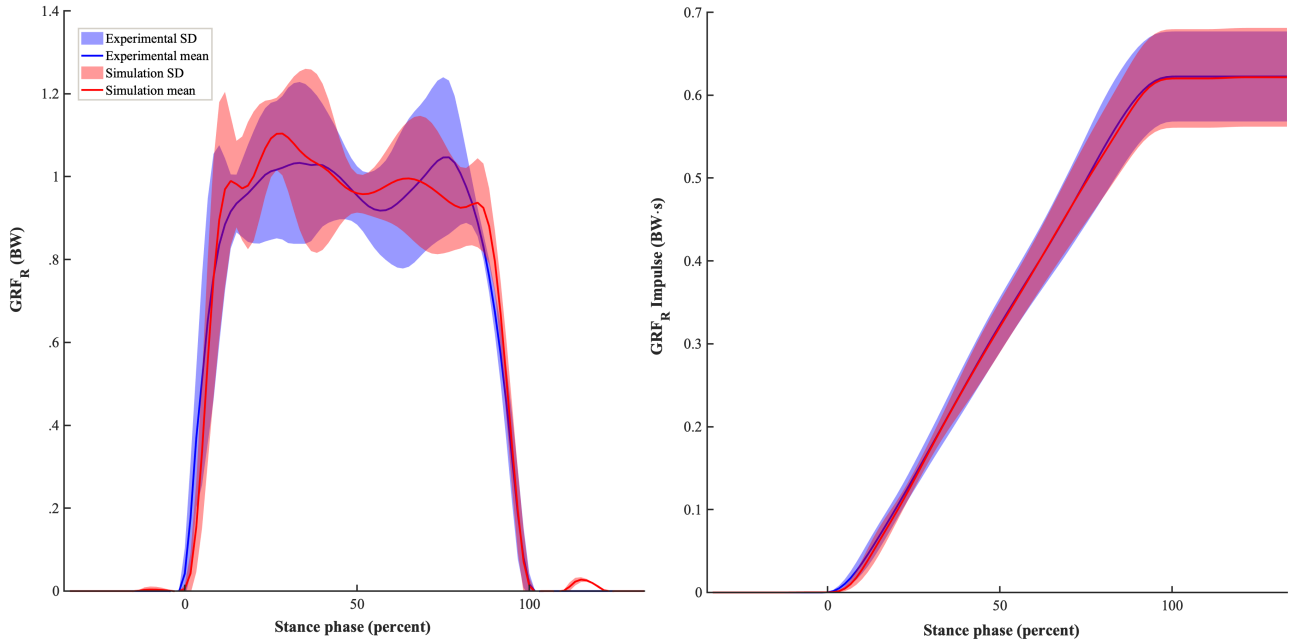

Figure 3: Optimized GRF_R (left) and GRF_R impulse (right) response for the medium stiffness trials. n = 4 trials.

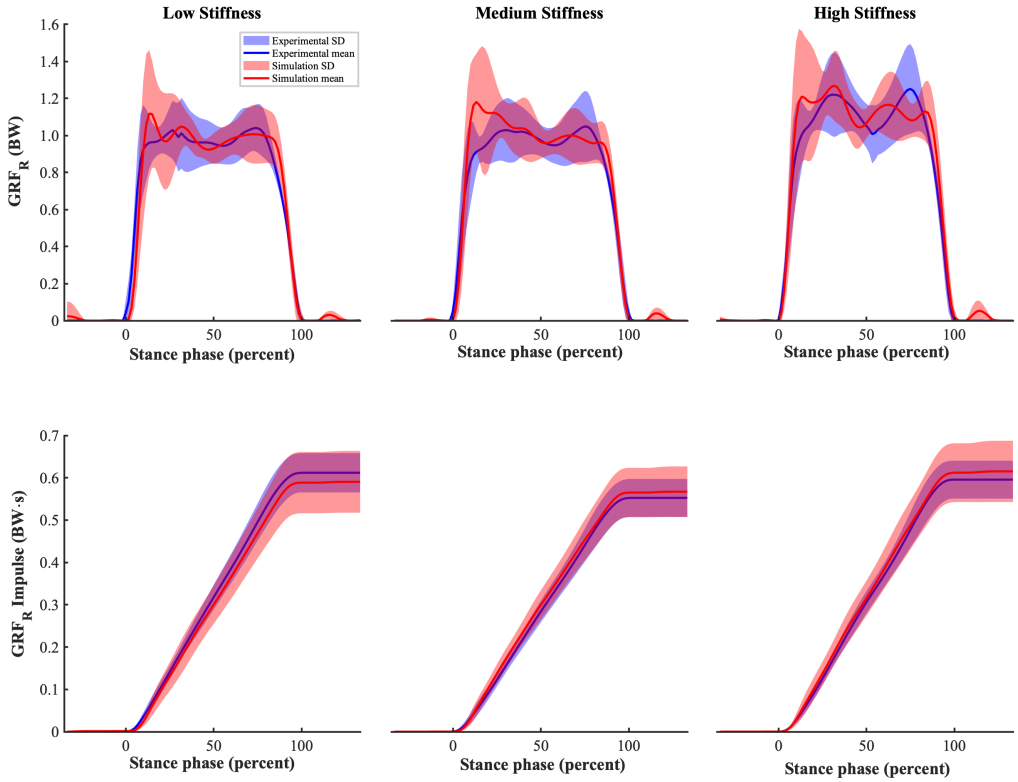

Figure 4: Ensemble curves (mean ± SD) for GRF_R (top) and GRF_R Impulse (bottom) for the low, medium, and high stiffness conditions (left, middle, and right). n = 34 trials.

Table 3: Summary of GRF_R, GRF_R impulse, and COP_{AP} comparison between simulated and experimental data.

Stiffness Configuration	GRF_R		GRF_R Impulse		COP_{AP}	
	R^2	RMSE (BW)	R^2	RMSE (BW·s)	R^2	RMSE (% FL)
Low	0.93 ± 0.04	0.12 ± 0.05	0.98 ± 0.06	0.03 ± 0.03	0.79 ± 0.10	13 ± 3.2
Medium	0.93 ± 0.09	0.11 ± 0.05	0.99 ± 0.01	0.02 ± 0.01	0.73 ± 0.16	15 ± 3.8
High	0.93 ± 0.02	0.12 ± 0.01	0.99 ± 0.01	0.02 ± 0.01	0.73 ± 0.22	14 ± 5.6

BW: Body weight, **COP_{AP}**: Anterior-posterior center of pressure, **FL**: Foot length, Data are mean ± SD

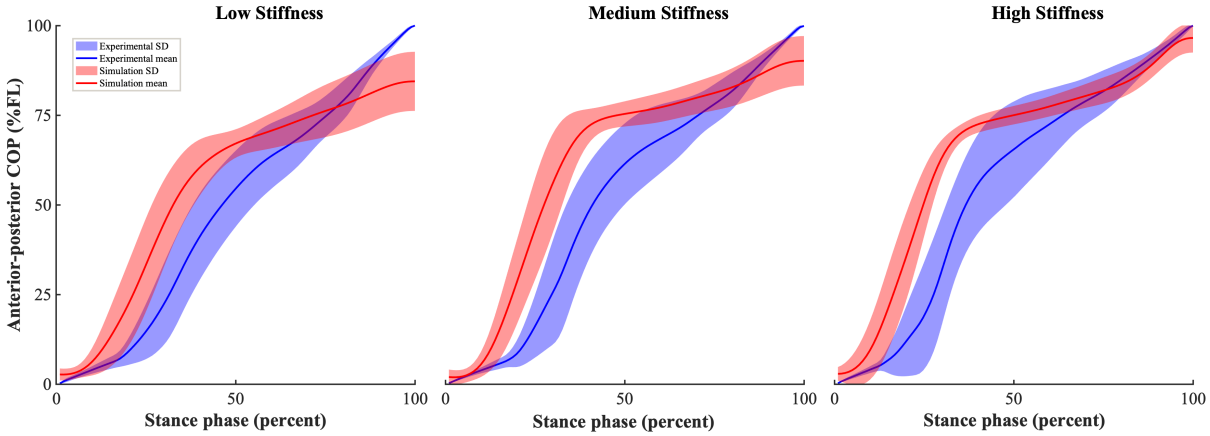

Figure 5: Ensemble curves for COP_{AP} position for the low, medium, and high stiffness conditions (left, middle, and right). **FL**: foot length. n = 34 trials.